ChemElectroChem

Research Article
doi.org/10.1002/celc.202200681

Chemistry Europe
European Chemical Societies Publishing

www.chemelectrochem.org

Special Collection

Monitoring the Dissolution and Hydrolysis of Pyrosulfate by Electrochemistry at a Liquid-Liquid Microinterface Array

Terence G. Henares,[a] Julian D. Gale,[a, b] Grégoire Herzog,[c] and Damien W. M. Arrigan*[a]

Dissolution and hydrolysis processes are important in a variety of settings, including industrial and environmental applications. In this work, the hydrolysis of pyrosulfate (disulfate) was investigated by ion-transfer electrochemistry at an array of microinterfaces between two immiscible electrolyte solutions (μITIES). Current associated with pyrosulfate transfer was observed, but it decreased with time. This is due to the hydrolysis of pyrosulfate to hydrogen sulfate and sulfate. Corroborating data for the hydrolysis was obtained from pH measurements (acidification of the aqueous solution) and Raman spectroscopy (formation of sulfate and hydrogen sulfate). Measurement of the ion-transfer potential from the voltammograms enabled estimation of pyrosulfate's Gibbs energy of transfer between the phases. Quantum mechanical calculations were employed to estimate the thermodynamics for the reactions of pyrosulfate, hydrogen sulfate and sulfate, which supported the experimentally observed trends. Altogether, these results illustrate the use of electrochemistry at the μITIES to characterise dissolution and hydrolysis processes.

Introduction

Dissolution of solids is an important spontaneous process involved in a multitude of applications such as pharmaceutical drug release, corrosion, and metal aerosol deposition into the oceans.[1–3] These solid-liquid processes can be classified into various physical events, for instance, particle wetting, solid breakdown, solvation, diffusion and convection. However, in some cases, the dissolution process is accompanied by a chemical reaction. Hydrolysis is one such chemical process which can accompany dissolution and entails solute cleavage by addition of water, under acidic or alkaline conditions, or in the presence of an enzyme, to form simpler molecules. Since hydrolysis can occur on the order of seconds, simple, sensitive and inexpensive analytical methods that can reveal information about the target compound are of practical importance.

Electrochemistry at the interface between two immiscible electrolyte solutions (ITIES) has been a well-established field for many decades.[4–6] The polarised ITIES, via an externally applied potential difference, serves as an interface to register an electrical current associated with the movement of ions across the interface. Electrochemistry at the ITIES has been employed in various investigations, including extraction chemistry, chemical and biochemical sensing, catalysis, biomembranes, particle behaviour, and energy storage.[7–10] For example, Girault's group have investigated the reduction of aqueous-phase oxygen by organic-phase decamethylferrocene (DMFc) at the water | 1,2-dichloroethane interface.[11] The first step of this process was identified as hydrolysis, whereby the O–H bond of water was weakened by metal cations behaving as Lewis acids, releasing a proton that protonated DMFc (DMFc-H^+). Subsequently, the participation of DMFc-H^+ in dioxygen reduction was observed as the interfacial transfer of $DMFc^+$ using cyclic voltammetry (CV) at the ITIES. Miniaturisation of the ITIES, e.g., to micro- or nanoscale, brings advantages to the electrochemical performance by decreasing the capacitive current, enhancing mass transport flux, and minimising the effects of ohmic drop,[12] as well as enabling use of simpler electrochemical cells, such as two-electrode cells rather than traditional four-electrode cells. With these benefits, ion transfer electrochemistry at the ITIES has the scope to be an excellent tool to monitor a chemical event occurring after a dissolution process.

Pyrosulfate (disulfate, $S_2O_7^{2-}$), which is easily hydrolysed,[13] has an important role in various industrial processes, such as decomposition of ore materials and alloys, and the production of sulfuric acid.[14,15] Recently, it has been used as a catalyst for the conversion of hemicellulose from barley straw to reducing sugars such as xylose and galactose, which are potential substrates for the production of fuels, including renewable hydrogen.[16] As an oxyanion, it has been used to stabilise tetravalent palladium[17] and as a component of a catalyst, diarylammonium pyrosulfate,[18] for ester hydrolysis. Thus, pyrosulfate is used in a range of industrial processes and fundamental studies.

[a] Dr. T. G. Henares, Prof. J. D. Gale, Prof. D. W. M. Arrigan
School of Molecular and Life Sciences
Curtin University
GPO Box U1987, Perth, Western Australia, 6845, Australia
E-mail: d.arrigan@curtin.edu.au
[b] Prof. J. D. Gale
Curtin Institute for Computation
Curtin University
GPO Box U1987, Perth, Western Australia, 6845, Australia
[c] Dr. G. Herzog
Université de Lorraine
CNRS, LCPME, 54000 Nancy, France

Supporting information for this article is available on the WWW under https://doi.org/10.1002/celc.202200681

Special Collection An invited contribution to the Hubert Girault Festschrift.

We are interested in the behaviour and applications of electrochemistry at the ITIES for sensors and electroanalytical methods. Initially, pyrosulfate was of interest to us as a possible aqueous phase electrolyte anion. However, its spontaneous hydrolysis prevented its use in this way. The aim of this report is to present our investigations into the hydrolysis of pyrosulfate monitored by electrochemistry at the ITIES. A two-electrode electrochemical cell was employed with the aid of a microporous glass membrane serving as scaffold for the formation of a μITIES array. From the resulting electrochemical behaviour, in conjunction with pH, spectroscopic and quantum mechanical results, the Gibbs energies of ion transfer of pyrosulfate, hydrogen sulfate and sulfate were estimated.

Results and Discussion

The hydrolysis of pyrosulfate is a well-known chemical process that occurs rapidly in aqueous solution at room temperature to form sulfate and hydrogen ions (Equation 1).[13]

$$S_2O_7^{2-} + H_2O \rightarrow 2HSO_4^- \rightleftharpoons 2SO_4^{2-} + 2H^+ \quad (1)$$

Using electrochemistry at the ITIES, we investigated this process to see if any participants in these reactions could be detected and any of their properties determined, such as their transfer potentials and Gibbs energies of transfer. The formation of the pyrosulfate anion in aqueous solution is a product of $K_2S_2O_7$ (solid) dissolution in deionised water, followed by its instantaneous hydrolysis to form the hydrogen sulfate and sulfate anions. The ion transfer (IT) of these anions from water to organic phase could be observed by polarising the interface with an applied potential and measuring an electrical current whenever an anion (possible one or more of pyrosulfate, hydrogen sulfate or sulfate) transfers across the ITIES. Based on Equation 1, CVs at the ITIES early and late in the dissolution/hydrolysis process can be expected to be different, due to the transformation of pyrosulfate to sulfate.

pH monitoring

Initially, the dissolution of the $K_2S_2O_7$ salt in deionized water (equivalent to 0.05 M $K_2S_2O_7$ upon complete dissolution) was observed by monitoring the solution pH over time and with stirring at room temperature. Note that complete dissolution occurred within the 20 min observation time of these experiments. The initial dissolution pH was about 2.4 ($<$ 20 s after introducing solid $K_2S_2O_7$ into the aqueous medium), indicating that the hydrolysis of the pyrosulfate had already commenced the moment water reacted with the salt. As shown in Figure 1, the dissolution of the solid $K_2S_2O_7$ salt resulted in a significant decline in solution pH during the initial stage ($<$ 200 s) until it reached pH 1.9 at ca. 600 seconds, after which it maintained this relatively constant pH value. Based on this evidence, it was apparent that $S_2O_7^{2-}$ dissolution and hydrolysis resulted in an acidic solution, as expected from Eq. 1. The dashed line in Figure 1 is a fit to the first order kinetics for the hydrolysis of pyrosulfate, assuming instantaneous dissolution of the added solid. The rate constant derived from that data is ca. 4×10^{-3} s^{-1}, in comparison to the previously reported value of 1.3×10^{-2} s^{-1}.[19]

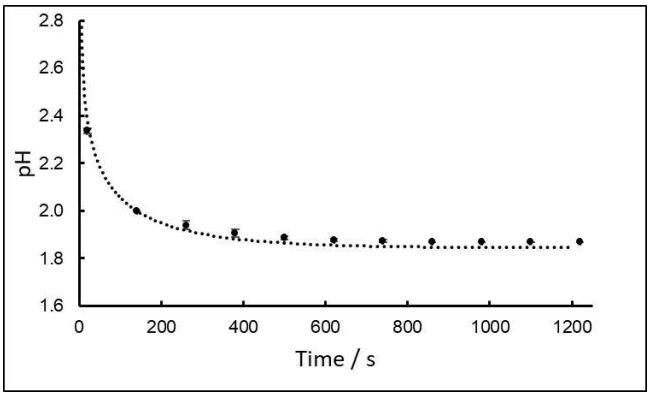

Figure 1. Monitoring of pH during the dissolution and hydrolysis of pyrosulfate in deionised water at room temperature. All data points are the average of three trials, with error bars of ± 1 standard deviation. The process was monitored continuously, with mass of material (ca. 65 mg) added to 50 mL of stirred de-ionised water. The dashed line shows the pH change for first order kinetics of the hydrolysis reaction.

Raman spectroscopy

To confirm the identity of the anions present during the hydrolysis of pyrosulfate in deionised water, Raman spectroscopy was employed. The characteristic Raman spectroscopic peaks for $S_2O_7^{2-}$, HSO_4^- and SO_4^{2-} occur at 1090 cm^{-1}, 1050 cm^{-1} and 981 cm^{-1}, respectively.[19] For the Raman spectroscopy measurements, we employed the dissolution of the $K_2S_2O_7$ salt to achieve a final concentration equivalent to 0.2 M, higher than the concentration used in the pH measurement experiments (0.05 M), because the lowest concentration that could be detected by Raman spectroscopy was ca. 0.01 M K_2SO_4 (Figure S1, supporting information). Although the anion concentration detectable was limited, simultaneous detection of multiple anions was possible. The dissolution of the $K_2S_2O_7$ salt was monitored at various time points. Based on the Raman spectral results, the disappearance of the $S_2O_7^{2-}$ anion peak and increases in the peaks for both HSO_4^- and SO_4^{2-} anions were observed (Figure 2). In these experiments, time zero was the time that deionised water was added into the spectrophotometric cuvette containing the solid $K_2S_2O_7$ salt; subsequently, the solution was mixed and spectroscopically monitored every 30 seconds. The initial dissolution spectral profiles revealed that the sample solution already contained pyrosulfate, HSO_4^- and SO_4^{2-} anions at the shortest time monitored – i.e., the formation of sulfate was sufficiently fast to be observable at the shortest time point, consistent with the pH monitoring study. The presence of hydrogen sulfate confirmed that the sample solution was acidic, which is consistent with the pH measurements (Figure 1). It is important to point out that the pKa of

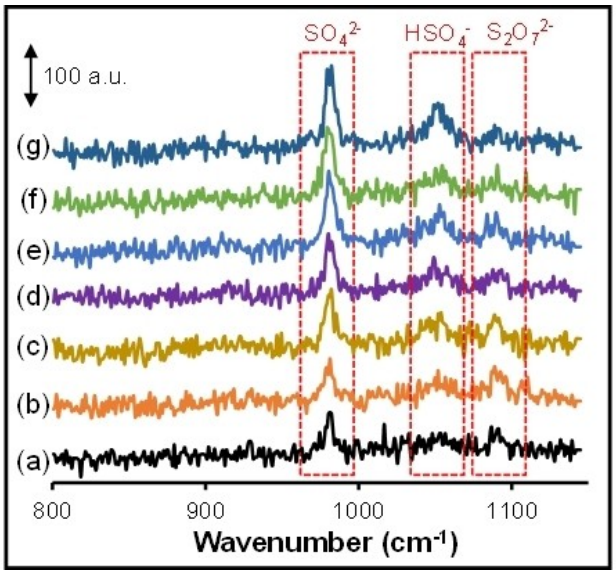

Figure 2. Raman spectra for the dissolution and hydrolysis of $K_2S_2O_7$ in deionised water at room temperature. Time points (min): (a) 0, (b) 0.5, (c) 1.0, (d) 1.5, (e) 2.0, (f) 2.5, (g) 3.0.

hydrogen sulfate is 1.99,[20] which implies that a solution with a pH close to the pKa value will show both the sulfate and hydrogen sulfate peaks in the Raman spectra, as observed here.

Electrochemistry at the μITIES array

Following the above confirmation of the dissolution and hydrolysis of pyrosulfate, electrochemistry at the ITIES was investigated as an approach to observe this process. The formal transfer potential of the anion $\Delta_o^w\Phi^{o'}$ depends on the formal Gibbs energy of transfer ($\Delta G_{tr}^{o',\,w\to DCE}$) which determines the preference of an ion for the aqueous phase or organic phase, as expressed in Eq. 2.[21]

$$\Delta G_{tr}^{o',\,w\to DCE} = zF\Delta_o^w\Phi^{o'} \quad (2)$$

The formal transfer potential $\Delta_o^w\Phi^{o'}$ can be determined experimentally by measuring the half-wave potentials of the target anion and of tetraethylammonium (TEA^+) cation.

Here, a glass micropore array was used to create the μITIES array. In this dissolution and hydrolysis process where formation of various anions occurs, it was important to monitor the stability of the Ag pseudo-reference electrode employed in the aqueous phase (Cells, 1, 2 and 3, Experimental Section). To do this, the ion transfer of 20 μM TEA^+ between water and organic phase was monitored during the dissolution and hydrolysis of $K_2S_2O_7$ in deionized water (Figure S2). The shape of the TEA^+ transfer CVs demonstrated two important points about the geometry of the ITIES. First, the forward scan (towards more positive potentials) showed a steady-state current associated with the transfer of TEA^+ from aqueous to organic phase, due to the formation of radial diffusion zones around the individual μITIES. Second, the reverse scan (towards more negative potentials) showed a peak current response signifying a linear diffusion process for the transfer of TEA^+ from organic to aqueous phase. These results were consistent with previously reported experiments and simulations[22] for transfers between aqueous and organic phases formed at these laser-ablated glass micropore membranes. During the hydrolysis of pyrosulfate, the half-wave potential for TEA^+ transfer shifted by about 30 mV towards lower potential. This shift is attributed to the change in composition of the aqueous phase during hydrolysis, as confirmed by the pH and Raman spectroscopy results; evidently the changing composition of ions, from pyrosulfate to hydrogen sulfate, sulfate and protons, interacted differently with the silver metal surface, altering the electrode potential slightly over time. Given the total run time of about 18 minutes, the potential changed at 1.6 mV min^{-1}.This minimal change indicates that analysis of the aqueous phase electrochemistry at the ITIES during dissolution and hydrolysis is feasible. In subsequent estimation of the transfer potential of pyrosulfate, this pseudo-reference electrode potential change was taken into account (see below), corresponding to an adjustment of ca. 1 mV for the timescale (ca. 40 s) between commencement of the experiment and appearance of the first voltammetric wave for pyrosulfate.

To provide an indication of the transfer potentials of sulfate and hydrogen sulfate, CVs with aqueous phases of 10 mM K_2SO_4 and 10 mM H_2SO_4 were conducted, i.e., Cells 2 and 3 (Figure 3). The CV for 10 mM H_2SO_4 in Figure 3 is undoubtedly due to a mixture of HSO_4^- and SO_4^{2-}; but with an excess of HSO_4^- and the expectation that HSO_4^- is less hydrophilic than SO_4^{2-}, this voltammogram is attributed to the transfer of HSO_4^-. Given the shapes of these CVs (Figure 3), measurement of the half-wave value potentials is challenging; accordingly, the foot potential (E_{foot}) approach was used. The E_{foot} was obtained as defined in Fig. S3. By comparing the E_{foot} values where the anion starts to move from aqueous to organic phase, the HSO_4^- anion commenced transfer at the more positive potential of $E_{foot} = -0.41$ V compared to SO_4^{2-} ($E_{foot} = -0.45$ V). This result suggests that the electrochemical cell could be used to differentiate the HSO_4^- and SO_4^{2-} anions and that the energy requirement for movement of HSO_4^- anion from aqueous to

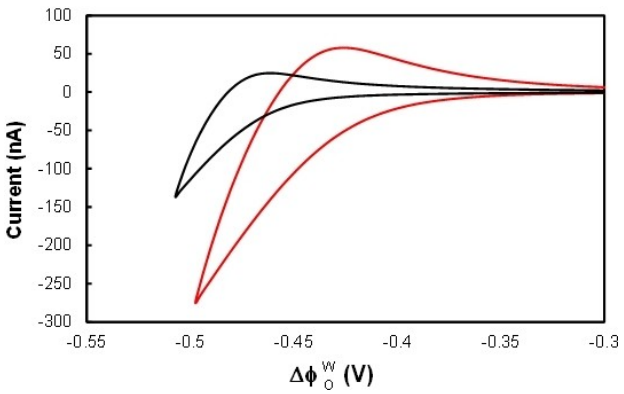

Figure 3. Cyclic voltammograms of the ITIES with aqueous phases of 10 mM K_2SO_4 (black line) or 10 mM H_2SO_4 (red line) solutions with compositions as given in Cell 2 or Cell 3 (Experimental Section), respectively. Scan rate: 10 mV s^{-1}.

organic phase was less than that for the SO_4^{2-} anion, as would be expected based on the typical trend for solvation energies with respect to the net charge of the ion. With the bulkier $S_2O_7^{2-}$ anion, we hypothesised that its transfer potential would be more evident during the initial stage of dissolution.

Figure 4 shows CVs for $K_2S_2O_7$ salt dissolution and hydrolysis of $S_2O_7^{2-}$ anion; an initial electrochemical response (red CV) was present that was attributed to the transfer of the $S_2O_7^{2-}$ anion, which is consistent with the Raman spectroscopic results that showed that the $S_2O_7^{2-}$ anion was present soon after dissolution but subsequently disappeared during hydrolysis. The shape of the CV attributed to pyrosulfate transfer in Figure 4 is consistent with an anion undergoing radial diffusion to the μITIES when transferring from aqueous to organic phase and undergoing linear diffusion in the organic phase (trapped in the pores) when transferring from organic to aqueous phase [as also seen for TEA^+ transfers (Figure S2)].[22] The data from pH and Raman spectroscopic measurements show that pyrosulfate disappears on reaction with water; the pH data (Figure 1) provided a hydrolysis rate of ca. $4\times10^{-3}\,s^{-1}$. This disappearance of pyrosulfate is also evident in the CVs (Figure 4; see also Figure S4, Supporting Information). The change in the ion-transfer currents with time indicates the decrease in pyrosulfate concentration and growth of hydrogen sulfate and sulfate concentrations. Both forward (aqueous to organic) and reverse (organic to aqueous) transfer currents decreased with time, albeit on a slower timescale than seen in the pH studies – this is attributed to the fact that the pH study solutions were stirred continuously whereas the CV experiments were not stirred but the aqueous phase was gently agitated between CV cycles. The formation of predominantly HSO_4^- anions could be deduced, due to the increase in acidity of the solution (as seen in the pH study).With an average E_{foot} of ca. −0.25 V for the $S_2O_7^{2-}$ anion compared to the E_{foot} of −0.41 V and −0.45 V for HSO_4^- and SO_4^{2-}, respectively, it is evident that the larger "di-tetrahedral" arrangement of pyrosulfate has a lower energy requirement for transfer across the ITIES. Unlike the HSO_4^- and SO_4^{2-} anions, it was straightforward to extract the Gibbs energy of transfer for $S_2O_7^{2-}$ anion since it has a well-defined voltammogram from which the half-wave potential can be determined. To calculate the transfer potential and Gibbs energy of transfer for both HSO_4^- and SO_4^{2-} anions, the half-wave potential was determined by using the difference between the E_{foot} value and the $E_{1/2}$ value for ideal voltammetric curves for mono- and divalent anions (Fig. S3). These $E_{1/2}$ values were equated to the formal transfer potentials $\Delta_o^w\Phi^{o'}$ of the HSO_4^- and SO_4^{2-} anions (Table 1) from which the Gibbs energies of transfer were estimated using Equation 2; the Gibbs energy of transfer for $S_2O_7^{2-}$ anion transfer ($\Delta G_{tr}^{o',\,w\to DCE}$) was estimated at 58 kJ mol^{-1} (see Table S1 for precision estimates).

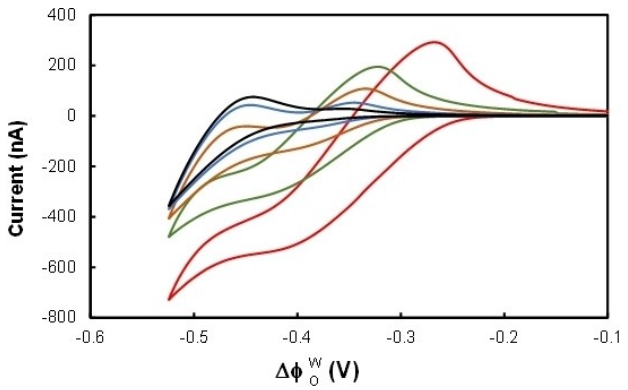

Figure 4. Cyclic voltammogram of the ITIES where the aqueous phase was the addition of solid $K_2S_2O_7$ to equivalent of 10 mM in deionized water. Monitoring time (seconds): 20 (red), 240 (green), 380 (orange), 500 (blue) and 620 (black). Other conditions as in Cell 3. Times indicate the start of the indicated scan after commencement of reaction. Scan rate: 10 mV s^{-1}.

As expected, the SO_4^{2-} anion has the largest $\Delta G_{tr}^{o',\,w\to DCE}$ with ~95 kJ mol^{-1} and is the most hydrophilic anion compared to $S_2O_7^{2-}$ and HSO_4^- anions. We note that the formal transfer potential of sulfate between water and 1,2-dichloroethane (DCE) was estimated at −0.8 V by Shioya et al.[23] whereas Cousens and Kucernak[24] reported a Gibbs free energy of transfer of 98 kJ mol^{-1}, equal to a formal transfer potential for sulfate of −0.51 V, in agreement with the findings here. The divalent anions, SO_4^{2-} and $S_2O_7^{2-}$, have substantial differences in transfer energy, which is likely to be due to the difference in anion size, with the $S_2O_7^{2-}$ anion having a lower charge/size ratio. Meanwhile, the monovalent HSO_4^- anion has a lower Gibbs energy of transfer compared to the divalent SO_4^{2-} anion, but is relatively close to that of $S_2O_7^{2-}$ anion.

Computational results

The solvation thermodynamics of the species considered above experimentally have also been examined through quantum mechanical calculations. For both water and 1,2-dichloroethane, the solvation free energy has been computed using the SMD continuum model. In the case of water, we also examined the influence of including explicit waters of hydration in order to more accurately describe the hydrogen bonding interactions. We note that the microhydration of both sulfate and hydrogen sulfate with small numbers of water molecules has been previously considered theoretically due to their significance for atmospheric chemistry.[25,26] For both sulfate and hydrogen sulfate, the anions were surrounded with 12 explicit waters of hydration, while for pyrosulfate[27] a total of 24 water molecules

Table 1. Estimated values of the Gibbs free energies of anion transfer.

Species	E_{foot} [V]	$\Delta_o^w\Phi^{o'}$ [V]	$\Delta G_{tr}^{o',\,w\to DCE}$ [kJ mol^{-1}]
SO_4^{2-}	−0.45	−0.49[a]	95
HSO_4^-	−0.41	−0.48[a]	46
$S_2O_7^{2-}$	–	−0.30[b]	58

[a] Transfer formal potentials are estimated from transfer foot potentials, assuming fully formed voltammograms of sulfate and hydrogen sulfate would have the same shape as the model voltammograms shown in Figure S3. [b]Transfer potential for pyrosulfate was adjusted for the shift in silver pseudo-reference electrode potential during the time from commencement of experiment to the time corresponding to the half-wave potential on the first voltammetric curve (Figure 4).

were included. The hydration free energies were then computed using the cluster method with the $(H_2O)_{12}$ cluster as the reference. The initial structure for this cluster prior to optimisation was taken from the Cambridge Cluster Database.[28] For pyrosulfate, we adopt the C_2 structure as proposed to be the ground state by Dyekjaer et al.[29]

Results for the computed solvation free energies are given in Table 2. As can be seen, explicit inclusion of water can lead to a substantial change in the hydration free energy varying between 15 and 100 kJ mol^{-1}. While this should make the values more accurate, we also note that there can be variation in the results depending on the exact number of water molecules chosen. In the case of sulfate and hydrogen sulfate there are literature estimates for the hydration free energies; Marcus[30] suggests values of −1080 and −330 kJ mol^{-1}, respectively, which agrees well with our current best values, except for a systematic offset of 60 kJ mol^{-1}. It should be noted that single ion solvation values are hard to define experimentally in an absolute sense as a choice has to be made as to how to partition the cation/anion contributions.

In the present study, the primary objective is to determine the thermodynamics of ion transfer between DCE and water, which can be equated with the transfer potential as determined electrochemically through the ITIES. Using the continuum solvent model values from Table 2, the free energies of transfer from water to DCE for sulfate, hydrogen sulfate and pyrosulfate are 188.5, 65.2 and 144.9 kJ mol^{-1}, respectively, which demonstrates good agreement with the trend observed experimentally in Table 1, although the values are all quantitatively overestimated. When introducing explicit hydration, the trend deviates for pyrosulfate as this value falls slightly below hydrogen sulfate, although the quantitative agreement is improved for all ions except sulfate. Besides the uncertainties in the theoretical method, there is a physical reason why the computed differences in solvation energies may tend to overestimate the transfer potential. This is because it is assumed that organic solvent is pure and that the ions transfer without their hydration shell. The present results suggest that it is likely that some degree of hydration may be retained when passing from water to DCE, as was reported for studies of cation[11] and anion transfers,[31] which would explain the reduction in transfer potential.

Besides the comparison with the transfer potential, we can use the theoretical data to compute two other relevant quantities. Firstly, the free energy for proton transfer from hydrogen sulfate to water can be determined, which can be related to the 2nd pKa for sulfuric acid. Treating the resulting hydronium ion as having an explicit first hydration shell of three water molecules leads to a pKa value of +0.1 in comparison to +1.99.[20] It is important to note that the exact prediction of pKa values is notoriously difficult and so an error of less than 2 represents good agreement. Secondly, we can predict the free energy for hydrolysis of pyrosulfate to hydrogen sulfate, which yields a value of −106.8 kJ mol^{-1}. While there is no experimental free energy available, to the best of our knowledge, this is in line with the experimental enthalpy of reaction, −87.65 kJ mol^{-1},[32] and the observed rapid hydrolysis of this anion in the presence of water.

Table 2. Solvation free energies (ΔG°) computed for water (hyd) and 1,2-dichloroethane (DCE) at the ωB97X-D3/ma-def2-QZVPP level of theory and the resultant free energies of transfer between water and DCE. Values were computed either with a continuum solvent model alone (SMD), or in the case of water with an explicit first solvent shell as well as a continuum description (Explicit + SMD).

Species	ΔG°_{hyd} (SMD) [kJ mol^{-1}]	ΔG°_{hyd} (Explicit + SMD) [kJ mol^{-1}]	ΔG°_{DCE} (SMD) [kJ mol^{-1}]	$\Delta G^{\circ, w-DCE}_{tr}$ (SMD) [kJ mol^{-1}]	$\Delta G^{\circ, w-DCE}_{tr}$ (Explicit + SMD) [kJ mol^{-1}]
SO_4^{2-}	−990.9	−1021.9	−802.4	188.5	219.5
HSO_4^-	−285.3	−270.2	−220.1	65.2	50.1
$S_2O_7^{2-}$	−823.5	−723.9	−678.6	144.9	45.3

Conclusions

This work presents the use of a simple μITIES array experiment to electrochemically monitor and extract estimated thermodynamic information from a dissolution process followed by hydrolysis. The dissolution of $K_2S_2O_7$ salt and hydrolysis of $S_2O_7^{2-}$ anion was characterised by not only this ion transfer electrochemical approach but also by Raman spectroscopy and pH measurements. The proton release during hydrolysis was confirmed by pH measurement while the disappearance of $S_2O_7^{2-}$ anion and formation of SO_4^{2-} and HSO_4^- anions were determined by Raman spectroscopy. This was further confirmed by the electrochemical investigation of the ion transfer potentials at the ITIES. The calculated Gibbs energy of anion transfer demonstrated that the SO_4^{2-} anion was the most hydrophilic compared to the $S_2O_7^{2-}$ and HSO_4^- anions and a similar trend in hydration and solvation energies was determined by quantum mechanical calculations. These results open up the possibility to use electrochemistry at the ITIES as a tool to study dissolution and hydrolysis processes of chemical or biochemical importance as well as demonstrating the importance of quantum mechanical calculations to support experimental studies of ion transfer processes (i.e., hydration, solvation and transfer energies).

Experimental Section

Reagents and materials

Reagents were purchased from Sigma-Aldrich Australia Ltd. except for potassium sulfate (Fluka), and all were used as received, unless otherwise specified. The organic electrolyte salt, bis(triphenylphosphoranylidene)ammoniumtetrakis(4-chlorophenyl)borate (BTPPATPBCl), was prepared by the metathesis of bis(triphenylphosphoranylidene)ammoniumchloride and potassium tetrakis(4-chlorophenyl)borate.[33] The organic phase electrolyte solution was 0.01 M BTPPATPBCl in 1,2-dichloroethane (DCE). Purified water with resistivity of 18.2 MΩ cm (Merck, Milli-Q Type 1 Ultrapure Water System) was used to prepare all aqueous solutions.

Microporous glass membranes were fabricated at the Australian National Fabrication Facility at the South Australia Node (ANFF-SA,

University of South Australia, Adelaide, South Australia) and the Optofab Node (ANFF-Optofab, Macquarie University, New South Wales).[22] Briefly, square arrays of 10×10 micropores were formed via laser ablation on a ~130 μm thick borosilicate glass substrate (13 mm diameter coverslips, type G402, Proscitech, Australia). The resulting laser entry and exit sides of the micropores had diameters of 53 μm and 23 μm, respectively. The vertical and horizontal pore centre-to-centre separations were 314 μm and the diagonal pore centre-to-centre separations were 447 μm. The membranes used in this work had their laser entry sides and pore internal walls treated with trichloro-(1*H*, 1*H*, 2*H*, 2*H*-perflourooctyl) silane to make them hydrophobic. In this way, the ITIES formed at the laser exit side, at the narrower pore openings.

Experimental methods

The dissolution and hydrolysis of potassium pyrosulfate ($K_2S_2O_7$) was monitored using pH measurements (laboratory pH meter CP-511, Elmetron, with a plastic combination pH electrode, Ionode Australia) and Raman spectroscopy (Olympus BX40). The experiments were conducted at room temperature and monitored at various time intervals. For pH measurements, the process was commenced by adding a known mass of salt to a known volume of de-ionised water, with continuous stirring. For Raman spectroscopy, a known mass of salt was placed in the clean dry spectroscopic cuvette and then a known volume of de-ionised water was added; the cuvette was agitated gently between measurements. The detection of pyrosulfate at the μITIES array was undertaken by cyclic voltammetry (CV) by adding a known mass of salt to the de-ionised water aqueous phase of known volume (Cell 1). The aqueous phase was agitated gently between measurements: the beaker containing the aqueous phase was gently moved in a horizontal circular fashion, on the benchtop, three times immediately after each CV cycle; then the whole cell was allowed to stand undisturbed for 30 s prior to commencement of the next CV cycle. Detection of sulfate and hydrogen sulfate was undertaken in solutions of specific concentrations of potassium sulfate and sulphuric acid, respectively (Cells 2 and 3). All electrochemical measurements were performed using an Autolab PGSTAT101N electrochemical system (Metrohm Autolab, Utrecht, The Netherlands) in conjunction with Metrohm's NOVA software. The electrochemical cells employed were as follows:

Cell 1: Ag | AgCl | 1 mM BTPPACl, 10 mM $LiCl_{(aq)}$ | 10 mM BTPPATPBCl, $DCE_{(org)}$ | | $K_2S_2O_{7(aq)}$ | Ag

Cell 2: Ag | AgCl | 1 mM BTPPACl, 10 mM $LiCl_{(aq)}$ | 10 mM BTPPATPBCl, $DCE_{(org)}$ | | 10 mM $K_2SO_{4(aq)}$ | Ag

Cell 3: Ag | AgCl | 1 mM BTPPACl, 10 mM $LiCl_{(aq)}$ | 10 mM BTPPATPBCl, $DCE_{(org)}$ | | 10 mM $H_2SO_{4(aq)}$ | Ag

The microporous glass membrane was connected to one end of a glass cylinder (internal diameter 7 mm) using an acetic acid curing silicone adhesive (Selleys, Australia & New Zealand). Then ca. 150 μL of organic electrolyte solution was placed into the glass membrane assembly which was then inserted into the aqueous phase (10 mL) followed by introduction of the organic reference solution (ca. 300 μL) on top of the organic electrolyte solution. Ag and Ag/AgCl electrodes were employed in the aqueous and organic reference solutions, respectively, as shown in Cells 1, 2 and 3. To calibrate the anion transfer potential, the tetraphenylarsonium tetraphenylborate assumption[34] was used to define the potential scale. The potential axis was calibrated by equating the experimental half-wave potential for tetraethylammonium (TEA^+) transfer to the formal transfer potential of TEA^+ at the water/DCE interface, 19 mV.[35] The experimental half-wave potential for 20 μM TEA^+ was measured directly from CVs. The half-wave potentials for the sulfate and hydrogen sulfate were estimated from the respective foot potentials (E_{foot}), defined as the potential at the foot of the voltammetric wave for anion transfer, because fully-formed voltammograms for the anions were not possible. An approach based on comparison of simulated voltammograms and incomplete experimental voltammograms for estimation of transfer potentials of species at the potential window limits was developed by Girault's group;[36,37] a similar approach based on comparison of ideal incomplete experimental voltammograms of the target ion was reported.[38] Use of the E_{foot} approach enabled comparison of behaviour of different species with incomplete voltammograms.[39] Here, we used the E_{foot} as a simple way to estimate the half-wave potential from an incomplete voltammogram, as described in Figure S3. Figure S3 illustrates the model voltammogram for reversible transfer of singly or doubly-charged anions and the resulting differences between E_{foot} and $E_{1/2}$. $E_{1/2}$ was used as the estimate of formal transfer potential. All experimentally determined thermodynamic values were estimations, since all sample solutions contained a mixture of two or more anions (at least millimolar) which affects the potential of the Ag pseudo-reference electrode employed in the aqueous phase. Drifts of the potential of the Ag pseudo-reference electrode due to the dissolution/hydrolysis of pyrosulfate were accounted for in the pyrosulfate potential measurements. The quality of each cell set-up was assessed by running CVs of TEA^+ transfer, which all indicated reversible, diffusion-controlled behaviour.

Computational methods

The thermodynamics of pyrosulfate, sulfate and hydrogen sulfate in both aqueous solution and 1,2-dichloroethane was determined using molecular quantum mechanical methods. All calculations were performed using density functional theory based on a long-range corrected hybrid functional[40] with empirical dispersion corrections and a large minimally augmented diffuse polarised quadruple-zeta basis set (ωB97X-D3/ma-def2-QZVPP). This level of theory has previously been shown to offer good performance for thermochemistry,[41] using the ORCA code, version 5.0.1.[42] All geometries were optimised initially in vacuum before being subsequently further relaxed in the presence of the SMD continuum model[43] using the parameters for the appropriate solvent. As is well documented in the literature, the use of a continuum model alone for water is often insufficient to obtain accurate results. Consequently, calculations were also performed in which explicit water molecules were included for the first hydration shell, in the case of aqueous solution, in addition to embedding within the SMD continuum solvent. Hydration free energies were then computed in the Ben-Naim standard state based on the cluster method of Bryantsev et al.[44] Vibrational frequencies were computed using analytic Hessians for all species *in vacuo* to ensure the absence of imaginary modes, and the corresponding zero-point energy and thermal corrections were applied to the free energies computed at 298.15 K.

Acknowledgements

This work was carried out with the support of the Australian Research Council (LP160100359, FL180100087). The Australian National Fabrication Facility (South Australia Node at University of South Australia; Optofab Node at Macquarie University) is thanked for fabrication of the glass micropore arrays used in this work. National Computational Infrastructure and the Pawsey Supercomputing Centre are acknowledged for the provision of computational resources. We thank Mr. Hum B. Lamichhane for

help with some experiments. Open Access publishing facilitated by Curtin University, as part of the Wiley - Curtin University agreement via the Council of Australian University Librarians.

Conflict of Interest

The authors declare no conflict of interest.

Data Availability Statement

The data that support the findings of this study are available from the corresponding author upon reasonable request.

Keywords: electrochemistry · hydrolysis · interfaces · ITIES · pyrosulfate

[1] J. B. Dressman, G. L. Amidon, C. Reppas, V. P. Shah, *Pharm. Res.* **1998**, *15*, 11–22.
[2] G. S. Frankel, *J. Electrochem. Soc.* **1998**, *145*, 2168–2198.
[3] N. M. Mahowald, D. S. Hamilton, K. R. M. Hackey, J. K. Moore, A. R. Baker, R. A. Scanza, Y. Zhang, *Nat. Commun.* **2018**, *9*, 2614.
[4] Z. Samec, *Pure Appl. Chem.* **2004**, *76*, 2174–2180.
[5] G. C. Gschwend, A. Olaya, P. Peljo, H. H. Girault, *Curr. Opin. Electrochem.* **2020**, *19*, 137–143.
[6] R. A. W. Dryfe, in *Adv. Chem. Phys.* S. A. Rice, editor, Wiley, New York, **2009**, vol. *141*, pp. 153–215.
[7] D. W. M. Arrigan, E. Alvarez de Eulate, Y. Liu, *Aus. J. Chem.* **2016**, *69*, 1016–1032.
[8] T. J. Stockmann, L. Angele, V. Brasiliense, C. Combellas, F. Kanoufi, *Angew. Chem. Int. Ed.* **2017**, *56*, 13493–13497.
[9] E. Laborda, A. Molina, V. F. Espin, F. Martinez-Ortiz, J. G. de la Torre, R. G Compton, *Angew. Chem. Int. Ed.* **2017**, *129*, 800–803.
[10] P. Peljo, M. Bichon, H. H. Girault, *Chem. Commun.* **2016**, *52*, 9761–9764.
[11] H. Q. Deng, T. J. Stockmann, P. Peljo, M. Opallo, H. H. Girault, *J. Electroanal. Chem.* **2014**, *731*, 28–35.
[12] S. Wilke, M. D. Osborne, H. H. Girault, *J. Electroanal. Chem.* **1997**, *436*, 53–64.
[13] H. K. Hofmeister, J. R. van Wazer, *Inorg. Chem.* **1962**, *1*, 811–812.
[14] I. M. Petrushina, N. J. Bjerrum, F. Cappeln, *J. Electrochem. Soc.* **1998**,*145*, 3721–3728.
[15] A. N. Ford, S. A. Tariq, *Microchem. J.* **1982**, *27*, 217–220.
[16] S. M. Butrim, T. D. Bil'dyukevich, N. S. Butrim, T. L. Yurkshtovich, *Russ. J. Appl. Chem.* **2010**, *83*, 134–138.
[17] J. Bruns, D. van Gerven, T. Kluner, M. S. Wickleder, *Angew. Chem. Int. Ed.* **2016**, *55*, 8121–8124.
[18] Y. Koshikari, A. Sakakura, K. Ishihara, *Org. Lett.* **2012**, *14*, 3194–3197.
[19] D. Littlejohn, K. Y. Hu, S. G. Chang, *Ind. Eng. Chem. Res.* **1988**, *27*, 1344–1348.
[20] S. Ilyas, H. Kim, R. R. Srivastava, *Sep. Purif. Technol.* **2021**, *254*, 117634.
[21] L. J. Sanchez Vallejo, J. M. Ovejero, R. A. Fernandez, S. A. Dassie, *Internat. J. Electrochem.* **2012** (2012) Art. ID 462197, doi: 10.1155/2012/462197.
[22] E. Alvarez de Eulate, J. Strutwolf, Y. Liu, K. O'Donnell, D. W. M. Arrigan, *Anal. Chem.* **2016**, *88*, 2596–2604.
[23] T. Shioya, S. Nishizawa, N. Teramae, *J. Am. Chem. Soc.* **1998**, *120*, 11534–11535.
[24] N. E. A. Cousens, A. R. Kucernak, *Electrochem. Commun.* **2011**, *13*, 1539–1541.
[25] D. S. Lambrecht, G. N. I. Clark, T. Head-Gordon, M. Head-Gordon, *J. Phys. Chem. A* **2011**, *115*, 11438–11454.
[26] D. E. Hussar, B. Temelso, A. L. Ashworth, G. C. Shields, *J. Phys. Chem. A* **2012**, *116*, 5151–5163.
[27] M. Abedi, H. Farrokhpour, S. Farnia, A. Najafi Chermahini, *J. Mol. Struct.* **2015**, *1093*, 125–134.
[28] The Cambridge Cluster Database, D. J. Wales, J. P. K. Doye, A. Dullweber, M. P. Hodges, F. Y. Naumkin F. Calvo, J. Hernández-Rojas, T. F. Middleton, http://www-wales.ch.cam.ac.uk/CCD.html.
[29] J. D. Dyekjaer, R. W. Berg, H. Johansen, *J. Phys. Chem. A* **2003**, *107*, 5826–5830.
[30] Y. Marcus, *Biophys. Chem.* **1994**, *51*, 111–127.
[31] R. Cui, Q. Li, D. E. Gross, X. Meng, B. Li, M. Marquez, R. Yang, J. L. Sessler, Y. Shao, *J. Am. Chem. Soc.* **2008**, *130*, 14364–14365.
[32] D. D. Wagman, W. H. Evans, V. B. Parker, R. H. Schumm, I. Halow, S. M. Bailey, K. L. Churney, R. L. Nuttall, *J. Phys. Chem. Ref. Data* **1982**, *11* (suppl. 2). https://srd.nist.gov/JPCRD/jpcrdS2Vol11.pdf.
[33] H. J. Lee, P. D. Beattie, B. J. Seddon, M. D. Osborne, H. H. Girault, *J. Electroanal. Chem.* **1997**, *440*, 73–82.
[34] A. J. Parker, *Chem. Rev.* **1969**, *69*, 1–32.
[35] T. Wandlowski, V. Mareček, Z. Samec, *Electrochim. Acta* **1990**, *35*, 1173–1175.
[36] M. D. Osborne, H. H. Girault, *Electroanalysis* **1995**, *7*, 425–434.
[37] Y. Shao, A. A. Stewart, H. H. Girault, *J. Chem. Soc. Faraday Trans.* **1991**, *87*, 2593–2597.
[38] M. Sairi, D. W. M. Arrigan, *Talanta* **2015**, *132*, 205–214.
[39] T. Osakai, Y. Yuguchi, E. Gohara, H. Katano, *Langmuir* **2010**, *26*, 11530–11537.
[40] Y.-S. Lin, G.-D. Li, S.-P. Mao, J.-D. Chai, *J. Chem. Theory Comput.* **2013**, *9*, 263–272.
[41] L. Goerigk, A. Hansen, C. Bauer, S. Ehrlich, A. Najibi, S. Grimme, *Phys. Chem. Chem. Phys.* **2017**, *19*, 32184–32215.
[42] F. Neese, F. Wennmohs, U. Becker, C. Riplinger, *J. Chem. Phys.* **2020**, *152*, 224108.
[43] A. V. Marenich, C. J. Cramer, D. G. Truhlar, *J. Phys. Chem. B* **2009**, *113*, 6378–6396.
[44] V. S. Bryantsev, M. S. Diallo, W. A. Goddard III, *J. Phys. Chem. B* **2008**, *112*, 9709–9719.

Manuscript received: June 21, 2022
Revised manuscript received: October 7, 2022
Accepted manuscript online: October 9, 2022